

# Cavity cooling of an optically levitated nanoparticle

Nikolai Kiesel,<sup>1,\*</sup> Florian Blaser,<sup>1,\*</sup> Uroš Delić,<sup>1</sup> David Grass,<sup>1</sup> Rainer Kaltenbaek,<sup>1</sup> and Markus Aspelmeyer<sup>1</sup>

<sup>1</sup>*Vienna Center for Quantum Science and Technology (VCQ), Faculty of Physics, University of Vienna, Boltzmannngasse 5, A-1090 Vienna, Austria*

The ability to trap and to manipulate individual atoms is at the heart of current implementations of quantum simulations [1, 2], quantum computing [3, 4], and long-distance quantum communication [5–8]. Controlling the motion of larger particles opens up yet new avenues for quantum science, both for the study of fundamental quantum phenomena in the context of matter wave interference [9, 10], and for new sensing and transduction applications in the context of quantum optomechanics [11, 12]. Specifically, it has been suggested that cavity cooling of a single nanoparticle in high vacuum allows for the generation of quantum states of motion in a room-temperature environment [13–15] as well as for unprecedented force sensitivity [16, 17]. Here, we take the first steps into this regime. We demonstrate cavity cooling of an optically levitated nanoparticle consisting of approximately  $10^9$  atoms. The particle is trapped at modest vacuum levels of a few millibar in the standing-wave field of an optical cavity and is cooled through coherent scattering into the modes of the same cavity [18, 19]. We estimate that our cooling rates are sufficient for ground-state cooling, provided that optical trapping at a vacuum level of  $10^{-7}$  millibar can be realized in the future, e.g., by employing additional active-feedback schemes to stabilize the optical trap in three dimensions [20–23]. This paves the way for a new light-matter interface enabling room-temperature quantum experiments with mesoscopic mechanical systems.

Cooling and coherent control of single atoms inside an optical cavity are well-established techniques within atomic quantum optics [24–28]. The main idea of cavity cooling relies on the fact that the presence of an optical cavity can resonantly enhance scattering processes of laser light that deplete the kinetic energy of the atom, specifically those processes where a photon that is scattered from the atom is Doppler-shifted to a higher frequency. It was realized early on that such cavity-enhanced scattering processes can be used to achieve laser cooling even of objects without exploitable internal level structure such as molecules and nanoparticles [18, 19, 29, 30]. For nanoscale objects, cavity cooling has been demonstrated in a series of recent experiments with nanobeams [31–33] and membranes of nm-

scale thickness (e.g. [34, 35]). To guarantee long interaction times with the cavity field these objects were mechanically clamped, which however introduces additional dissipation and heating through the mechanical support structure. As one consequence, quantum signatures have thus far only been observed in a cryogenic environment [36, 37]. Freely suspended particles can circumvent this limitation and allow for far better decoupling of the mesoscopic object from the environment. This has been successfully implemented for atoms driven at optical frequencies far detuned from the atomic resonances, both for the case of optically trapped single atoms [26, 27] and for clouds of up to  $10^5$  ultracold atoms [38–40]. In contrast to such clouds, massive solid objects provide access to a new parameter regime: on the one hand, the rigidity of the object allows to manipulate the center-of-mass motion of the whole system, thus enabling macroscopically distinct superposition states [14, 15, 41]; on the other hand the large mass density of solids concentrates many atoms in a small volume of space, which provides new perspectives for force sensing [16, 17]. In our work, we have now extended the scheme to dielectric nanoparticles comprising up to  $10^9$  atoms. By using a high-finesse optical cavity for both optical trapping and manipulation we demonstrate, for the first time, cavity-optomechanical control, including cooling, of the center-of-mass (CM) motion of a levitated solid object without internal level structure.

To understand the principle of our approach, consider a dielectric spherical particle of radius  $r$  smaller than the optical wavelength  $\lambda$ . Its finite polarizability  $\xi = 4\pi\epsilon_0 r^3 \text{Re} \left\{ \frac{\epsilon-1}{\epsilon+2} \right\}$  ( $\epsilon$ : dielectric constant;  $\epsilon_0$ : vacuum permittivity) results in an optical gradient force that allows to trap particles in the intensity maximum of an optical field [42]. The spatial modes of an optical cavity provide a standing-wave intensity distribution along the cavity axis  $x$ . A nanoparticle that enters the cavity will be pulled towards one of the intensity maxima, located a distance  $x_0$  from the cavity center. For the case of a Gaussian (TEM00) cavity mode, the spatial profile will result in radial trapping around the cavity axis, hence providing a full 3D particle confinement. In addition, Rayleigh scattering off the particle into the cavity mode induces a dispersive change in optical path length and shifts the cavity resonance frequency by  $U_0(x_0) = \frac{\omega_{cav}\xi}{2\epsilon_0 V_{cav}} \left( 1 + \frac{x_0^2}{x_R^2} \right)$  [43] ( $\omega_{cav}$ : cavity frequency;  $V_{cav}$ : cavity mode volume;  $x_R$ : cavity-mode Rayleigh length). This provides the underlying optomechanical coupling mechanism between the CM motion of a particle moving along the cavity axis and the photons of a Gaussian cavity mode. The result-

\*These authors contributed equally to this work.

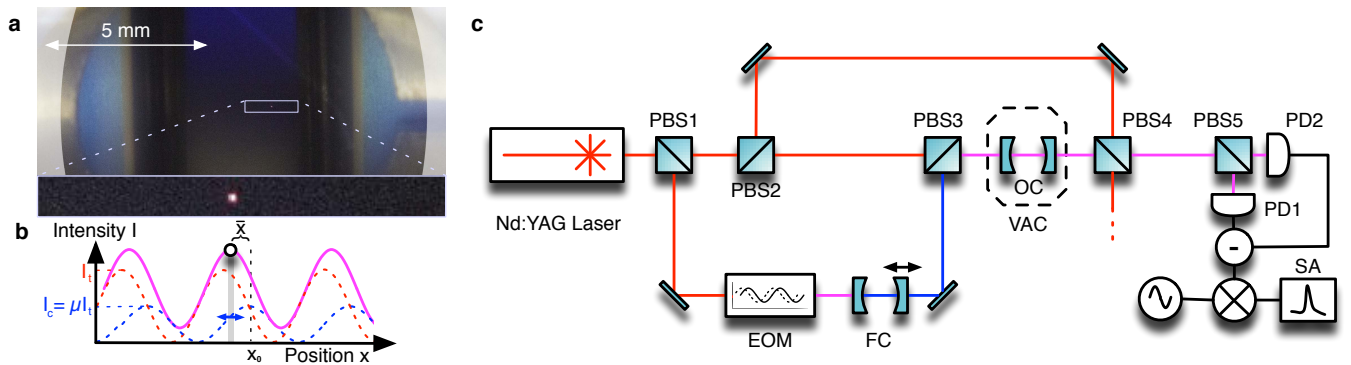


FIG. 1: **Optical trapping and readout of a nanoparticle in a Fabry-Perot cavity.** (a) **Nanoparticle in a cavity.** A photo of our near-confocal Fabry-Perot optical cavity (OC) ( $F=76000$ ;  $L = \frac{c}{2\text{FSR}} = 10.97$  mm, determined via the free spectral range FSR). The white-shaded areas indicate the curvature of the cavity mirrors. The optical field between the mirrors traps a nanoparticle. The enlarged inset shows light scattered by the nanoparticle. (b) **Schematics of two-mode optical trap and dispersive coupling.** Two optical fields form standing-wave intensity distributions along the optical cavity axis (dashed lines; blue: control beam; red: trapping beam). Because of their different frequencies, the intensity maxima of the two fields are displaced with respect to each other. A nanoparticle is trapped at the maximum of the total intensity distribution (purple solid line). Since the trapping beam is more intense than the control beam, the nanoparticle is trapped at a distance  $\bar{x} \neq 0$  away from the control-beam intensity maximum  $x_0$ . As a consequence, the nanoparticle oscillates within a region where the control-beam intensity varies with the particle position (blue arrow), resulting in linear dispersive coupling (see main text and appendix). The displacement  $\bar{x}$  depends on the ratio between the intensity maxima of the two fields (c) **Experimental setup.** A Nd:YAG laser ( $\lambda = 1064$  nm) is split into three beams at the polarizing beam splitters PBS1 and PBS2 (for simplicity waveplates not shown in the figure). The transmitted beam is used to lock the laser to the TEM00 mode of the OC and provides the trapping field for the nanoparticle. The beam reflected at PBS1 is used to prepare the control beam, which is frequency-shifted by  $\delta\omega$  close to the adjacent cavity resonance of the TEM00 mode, i.e.,  $\delta\omega = \text{FSR} + \Delta$  ( $\Delta$ : detuning from cavity resonance). The single-frequency sideband at  $\delta\omega$  is created using an electro-optical modulator (EOM) followed by optical amplification in fiber (not shown) and transmission through a filtering cavity (FC) with an FWHM linewidth of  $2\pi \times 500$  MHz. The control and trapping beams are overlapped at PBS3 and transmitted through the OC with orthogonal polarizations. The OC is mounted inside a vacuum chamber (VAC). When a nanoparticle is trapped in the optical field in the cavity, its center-of-mass (CM) motion introduces a phase modulation on the control beam. To detect this signal, we perform interferometric phase readout of the control beam: At PBS4 the trapping beam is separated from the control beam and overlapped with the local oscillator (LO). After rotating the polarization, the control beam and the LO are mixed at PBS 5. High-frequency InGaAs photo detectors PD1 and PD2 detect the light in both output ports of PBS5. We mix the difference signal of the two detectors with an electronic local oscillator of frequency  $\text{FSR} + \Delta$  and record the noise power spectrum of resulting signal at a spectrum analyzer (SA) (see Methods).

ing interaction Hamiltonian is

$$H_{int} = -\hbar U_0(x_0) \hat{n} \sin^2(kx_0 + k\bar{x} + k\hat{x}),$$

where we have allowed for a mean displacement  $\bar{x}$  of the nanoparticle with respect to the intensity maximum  $x_0$  ( $\hat{x}$ : CM position operator of the trapped nanoparticle;  $k = \frac{2\pi}{\lambda}$ : wavenumber of the cavity light field;  $\hat{n}$ : cavity photon number operator). For the case of a single optical cavity mode, the particle is trapped at an intensity maximum ( $\bar{x} = 0$ ) and, for small displacements, only coupling terms that are quadratic in  $\hat{x}$  are relevant [34]. Linear coupling provides intrinsically larger coupling rates and can be exploited for various quantum control protocols [44]. However, it requires to position the particle outside the intensity maximum of the field. This can be achieved for example by an optical tweezer external to the cavity [14], by harnessing gravity in a vertically mounted cavity [45] or by using a second cavity mode with longitudinally shifted intensity maxima [13, 14].

We follow the latter approach and operate the optical

cavity with two longitudinal Gaussian modes of different frequency, namely, a strong “trapping field” to realize a well-localized optical trap at one of its intensity maxima, and a weaker “control field” that couples to the particle at a shifted position  $\bar{x} \neq 0$ . For localization in the Lamb-Dicke regime ( $k^2 \langle \hat{x}^2 \rangle \ll 1$ ) this yields [12, 46] linear optomechanical coupling between the trapped particle and the control field at a rate  $g_0 = U_0(x_0) \sin(2k\bar{x}) k \sqrt{\frac{\hbar}{m\Omega_0}}$  per photon ( $m$ : nanoparticle mass;  $\Omega_0$ : frequency of CM motion). Detuning of the control field from the cavity resonance by a frequency  $\Delta = \omega_{cav} - \omega_c$  ( $\omega_c$ : control field frequency) results in the well-known dynamics of cavity optomechanics [12]. Specifically, the position dependence of the gradient force will change the stiffness of the optical trap, shifting  $\Omega_0$  to an effective frequency  $\Omega_{\text{eff}}$  (optical spring), and the cavity-induced retardation of the force will introduce additional optomechanical (positive or negative) damping on the particle motion. From a quantum-optics viewpoint, the oscillating nanoparti-

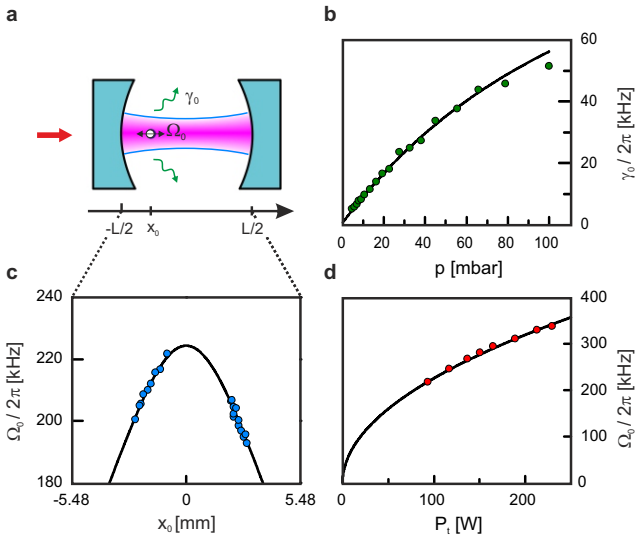


FIG. 2: **Experimental characterization of the nanoparticle cavity trap.** (a) **Schematic of the trap configuration.** An optical cavity of length  $L = 10.97$  mm is driven on resonance of a Gaussian TEM00 cavity mode by a laser with a wavelength of  $\lambda = 1064$  nm. The nanoparticle is optically trapped at position  $x_0$ . Its center-of-mass motion in the axial direction of the cavity is described by a harmonic oscillator with a frequency  $\Omega_0$  and an amplitude of approximately 10 nm. In addition, the nanoparticle experiences collisions with the surrounding gas resulting in a damping rate  $\gamma_0$ . (b) **Mechanical damping  $\gamma_0$  as a function of pressure.** The solid line is a fit of kinetic gas theory to the data (see appendix D). (c) **Position-dependent trapping frequency.** The waist of the optical mode expands from approximately  $41\mu\text{m}$  at the cavity center to  $61\mu\text{m}$  at the cavity mirrors, resulting in a position-dependent trapping potential. Here, we show the corresponding change of the trapping frequency  $\Omega_0$  with the position of the nanoparticle. (d) **Power-dependent trapping frequency.** We experimentally show the dependence of the trapping frequency on the intracavity power  $P_t$ . The solid lines in Fig. c, d are based on the theoretical model as described in the main text, with a scaling factor as the only free fit parameter.

cle scatters photons into optical sidebands of frequencies  $\omega_c \pm \Omega_0$  at rates  $A_{\pm} = \frac{1}{4} \frac{g_0^2 \langle \hat{n} \rangle \kappa}{(\kappa/2)^2 + (\Delta \pm \Omega_0)^2}$ , known as Stokes and anti-Stokes scattering, respectively ( $\kappa$ : FWHM cavity linewidth). For  $\Delta > 0$  (red detuning) anti-Stokes scattering becomes resonantly enhanced by the cavity, effectively depleting the kinetic energy of the nanoparticle motion via a net laser-cooling rate of  $\Gamma = A_- - A_+$ . In the following, we demonstrate all these effects experimentally with an optically trapped silica nanoparticle.

As is shown in Figure 1, our setup comprises a high-finesse Fabry-Perot cavity (Finesse  $F = 76000$ ;  $\kappa = 2\pi \times 180$  kHz) that is mounted inside a vacuum chamber kept at a pressure between 1 and 5 mbar. Airborne silica nanoparticles (specified with radius  $r = 127 \pm 13$  nm) are emitted from an isopropanol solution via an ul-

trasonic nebulizer and are trapped inside the cavity in the standing wave of the trapping field (see Methods Section). To achieve the desired displacement between the intensity maxima of trapping field and control field ( $\bar{x} \neq 0$ ), we use the adjacent longitudinal cavity mode for the control beam, i.e. the cavity mode shifted by approximately one free spectral range  $\text{FSR} = \frac{c}{2L} \approx 13.67$  GHz in frequency from the trapping beam ( $c$ : vacuum speed of light;  $L$ : cavity length). Depending on the distance from the cavity center  $x_0$ , the two standing-wave intensity distributions are then shifted with respect to each other by  $\frac{\lambda}{2L}(x_0 + L/2)$  (Figure 1c). For example, to achieve maximal coupling  $g_0$  for weak control beam powers, i.e. for  $\mu = \frac{P_c}{P_t} \ll 1$  ( $P_{c(t)}$ : Power of control (trapping) beam in the cavity), the nanoparticle needs to be positioned at  $x_0 = L/4$ , where the antinodes of the two beams are separated by  $\lambda/8$  [13, 14]. Note that when the control beam is strong enough to significantly contribute to the optical trap ( $\mu \gtrsim 0.1$ ), the displacement  $\bar{x}$  and both  $\Omega_0$  and  $g_0$  are modified when  $\mu$  is changed [39]. The exact dependence of these optomechanical parameters on  $\mu$  depends on  $x_0$  (see appendix A and [47, 48]).

The optomechanical coupling between the control field and the particle can be used to both manipulate and detect the particle motion. Specifically, the axial motion of the nanoparticle generates a phase modulation of the control field, which we detect by heterodyne detection (see methods section). We reconstruct the noise power spectrum (NPS) of the mechanical motion by taking into account the significant filtering effects exhibited by the cavity (arising from the fact that  $\kappa \approx \Omega_0$ ) on the transmitted control beam ([49] and appendix A). The inferred position sensitivity of our readout scheme for a nanoparticle of approx. 170 nm radius is  $4 \text{ pm}/\sqrt{\text{Hz}}$ , which is likely limited by classical laser noise (see below).

The properties of our optical trap are summarized in Figure 2. The influence of the control beam on the trapping potential is purposely kept small by choosing  $\mu \approx 0.1$  and  $\Delta \approx 0$ . We expect that the axial mechanical frequency  $\Omega_0$  depends both on the power of the trapping beam  $P_t$  and on  $x_0$  through the cavity beam waist  $W(x_0)$  via  $\Omega_0 = \sqrt{\frac{12k^2}{c\pi} \text{Re}\left(\frac{1}{\rho} \frac{\epsilon-1}{\epsilon+2}\right)} \cdot \sqrt{\frac{P_t}{\pi W(x_0)}}$  [13, 14], in agreement with our data. The damping  $\gamma_0$  of the mechanical resonator is dominated by the ambient pressure of the background gas down to a few millibar (Fig. 1c). Below these pressures the nanoparticle is not stably trapped anymore, while trapping times up to several hours can be achieved at a pressure of a few millibar. This is a known, yet unexplained phenomenon [21, 22, 47]. Reproducible optical trapping at lower pressure values has thus far only been reported using feedback cooling in three dimensions for the case of nanoparticles [21, 22] or, without feedback cooling, with particles of at least  $20\mu\text{m}$  radius [50].

We finally demonstrate cavity-optomechanical control of our levitated nanoparticle. All measurements have been performed with the same particle for an intra-cavity trapping beam power  $P_t$  of approx. 55 W and at a pres-

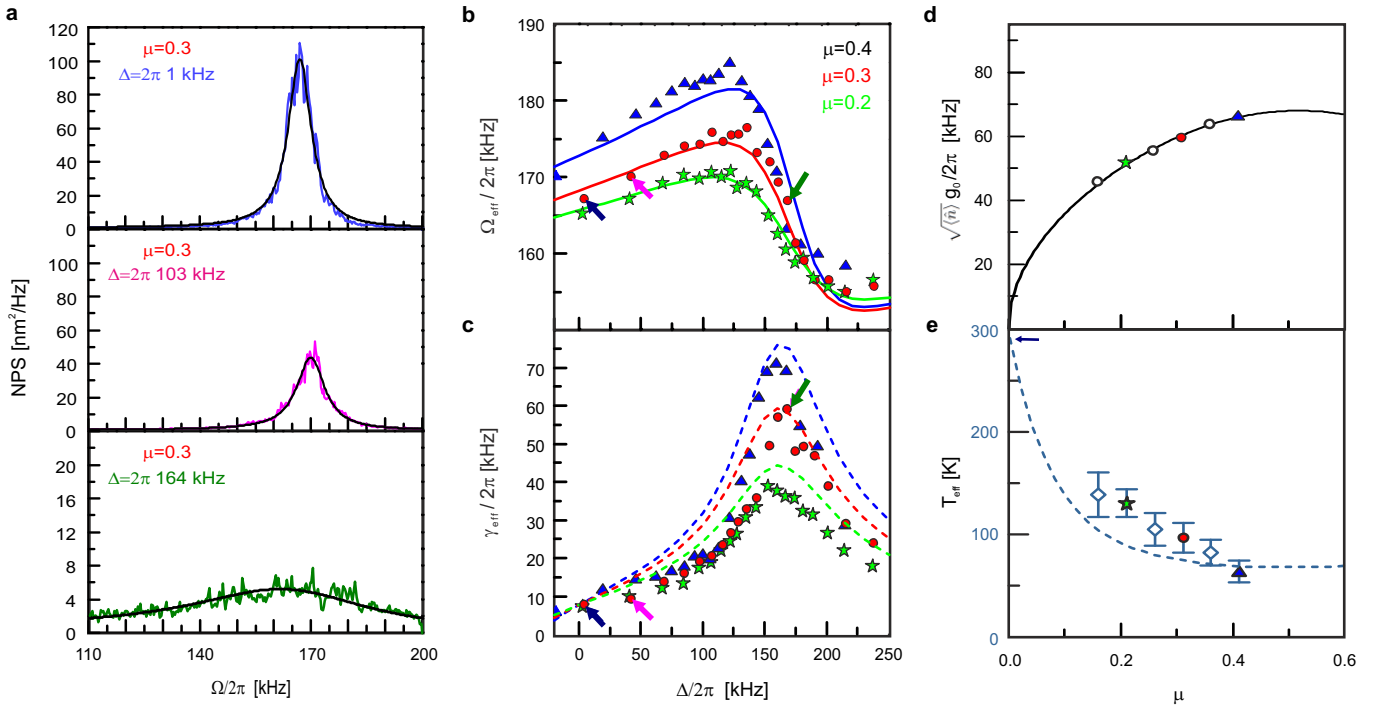


FIG. 3: **Cavity-optomechanical control and cooling of a nanoparticle.** We obtain noise power spectra (NPS, see panel (a)) of the nanoparticle’s center-of-mass motion for different settings of the control-beam power  $P_c$  and detuning  $\Delta$ . During each measurement,  $\mu = \frac{P_c}{P_t}$  was kept constant ( $P_t$ : trapping beam power). Based on these NPS, we determine the effective mechanical frequency  $\Omega_{\text{eff}}$  and linewidth  $\gamma_{\text{eff}}$  of the optomechanical system, and its effective temperature  $T_{\text{eff}}$ . We study the modification of these spectra caused by optomechanical interaction in panels (b), (c) and (e). Based on the data in panel (b) we infer the power-dependent strength of optomechanical coupling in panel (d). **(a) Mechanical noise power spectra.** Shown are examples of the mechanical NPS measured for constant control-beam power ( $\mu = 0.3$ ) at three different detunings  $\Delta$  with respect to the cavity resonance frequency. The detuning results in a significant modification of the NPS due to optomechanical effects. Note that scale is changed by a factor of 5 in the bottom plot in panel (a). In order to determine the effective mechanical frequency  $\Omega_{\text{eff}}$  and linewidth  $\gamma_{\text{eff}}$  of the optomechanical system, we fit the NPS of an harmonic oscillator (black solid lines) to this data. We infer the value of the effective temperature  $T_{\text{eff}}$  from the equipartition theorem via direct integration of the NPS (see appendix C). **(b) Optical spring.** When the control beam is red-detuned from the cavity resonance ( $\Delta > 0$ ), we observe a characteristic modification of the mechanical frequency  $\Omega_{\text{eff}}$ . The solid lines in (b) correspond to a theoretical model that is fitted to the data for each value of  $\mu$ . The optomechanical coupling  $g_0\sqrt{\langle\hat{n}\rangle}$  is one of the fit parameters (see appendix C). Based on these results for the optical spring, we calculate the theoretical expectations for  $\gamma_{\text{eff}}$  and  $T_{\text{eff}}$ , which are shown as dashed lines in panels (c) and (e). **(c) Optomechanical damping.** Linewidth broadening of the mechanical resonance as a function of the detuning  $\Delta$ . **(d) Optomechanical coupling.** We infer the optomechanical coupling rate  $g_0\sqrt{\langle\hat{n}\rangle}$  from the strength of the optical spring (panel (b)) and show its dependence on the power ratio  $\mu$ . This relation depends on the position  $x_0$  of the nanoparticle in the cavity. For the data presented here, we determine  $x_0 = 1.56 \pm 0.14$  mm (see appendix E). We find very good agreement between the data and the theoretical model, where only the nanoparticle polarizability serves as a fit parameter (solid line; also see appendix C). **(e) Cavity cooling.** The decrease in effective temperature  $T_{\text{eff}}$  is shown for increasing control-beam power. To obtain a good estimate of the measurement error, we average over measurements taken for detunings between  $\Delta = 100 - 150$  kHz (see appendix C). The dashed line is a theoretical prediction based on the parameters obtained from the fit to the optical spring data (panel (b)).

sure of  $p \approx 4$  mbar. This corresponds to a bare mechanical frequency  $\Omega_0/2\pi = 165 \pm 3$  kHz and an intrinsic mechanical damping rate  $\gamma_0/2\pi = 7.2 \pm 0.8$  kHz, respectively. Figure 3a shows the dependence of a typical noise power spectrum (NPS) of the particle’s motion upon detuning of the control field. Note that the power ratio  $\mu$  between trapping beam and control beam is kept constant, which is achieved by adjusting the control-beam power for different detunings. The amplitude scale, as well as the temperature scale in Figure 3e, is calibrated

through the NPS measurement performed close to zero detuning ( $\Delta = 1$  kHz; blue NPS in Fig. 3a by using the equipartition theorem for  $T = 293\text{K}$ ). This is justified by an independent measurement that verifies thermalization of the center of mass (CM) mode at zero detuning for our parameter regime (see appendix D). Both the inferred effective mechanical frequency  $\Omega_{\text{eff}}$  (Figure 3b) and the effective mechanical damping  $\gamma_{\text{eff}}$  (Figure 3c) show a systematic dependence on the detuning  $\Delta$  of the control beam, in good agreement with the ex-

pected dynamical backaction effects for linear optomechanical coupling (see appendix A). A fit of the expected theory curve to the optical spring data allows estimating the strength of the optomechanical coupling for different values of  $\mu$  (Figure 3d). If the position  $x_0$  of the nanoparticle in the cavity is known, then this behaviour is uniquely determined by  $U_0(x_0)$ . For a particle position  $x_0 = 1.56 \pm 0.14$  mm, which was determined independently with a CCD camera, we find  $U_0(x_0) = 2\pi \times (145 \pm 2)$  kHz. These values allow to infer a nanoparticle displacement  $\bar{x} \approx 0.15 \times (\lambda/2) = 77$  nm, yielding a fundamental single-photon coupling rate  $g_0 \approx 2\pi \times 1.2$  Hz (for  $\mu \rightarrow 0$ ). Assuming a (supplier specified) material density of  $\rho = 1950$  g/cm<sup>3</sup> and a dielectric constant  $\epsilon_{\text{SiO}_2} = 2.1$ , our results indicate a single trapped nanoparticle of radius  $r \approx 169$  nm.

The red-detuned driving of the cavity by the control laser also cools the CM motion of the levitated nanoparticle through coherent scattering into the cavity modes. Figure 3e shows the resulting effective temperature as deduced from the area of the NPS of the mechanical motion by applying the equipartition theorem. The experimental data is well in agreement with the expected theory for cavity cooling (see appendix A). We achieve cooling rates of up to  $\Gamma = 2\pi \times 49$  kHz and effective optomechanical coupling rates of up to  $g_0 \sqrt{\langle \hat{n}_c \rangle} = 2\pi \times 66$  kHz ( $\langle \hat{n}_c \rangle$ : mean photon number in control field), comparable to state-of-the-art clamped mechanical systems in that frequency range [12]. The demonstrated cooling performance, with a minimal CM-mode temperature of  $64 \pm 5$  K, is only limited by damping through residual gas pressure that results in a mechanical quality of  $Q = \frac{\Omega_0}{\gamma_0} \approx 25$ . Recent experiments [21, 22] impressively demonstrate, that lower pressures can be achieved when cooling is applied in all three spatial dimensions. Given the fact that our cavity-induced longitudinal cooling rate is comparable to the feedback cooling rates achieved in those experiments, a combined scheme should eventually be capable of performing quantum experiments at moderately high vacuum levels. For example, our cooling rate is in principle sufficient to obtain cooling to the quantum ground state of the CM-motion starting from room temperature with a longitudinal mechanical quality factor of  $Q \approx 10^9$ , i.e., a vacuum level of  $10^{-7}$  mbar. Such a performance is currently out of reach for other existing cavity optomechanical systems with comparable frequencies. In addition, even larger cooling rates are expected when both beams are red-detuned to cooperatively cool the nanoparticle motion [47].

Our experiment constitutes a first proof of concept demonstration in that direction. We envision that once this level of performance is achieved levitated nanoparticles in optical cavities will provide a room-temperature quantum interface between light and matter, along the lines proposed in [13, 14, 44, 51], with new opportunities for macroscopic quantum experiments in a regime of large mass [15, 41, 52]. The large degree of optomechanical control over levitated objects may also enable

applications in other areas of physics such as for precision force sensing [16, 17] or for studying non-equilibrium dynamics in classical and quantum many-body systems [53].

## Acknowledgements

We would like to thank O. Romero-Isart, A. C. Pflanzner, J. I. Cirac, P. Zoller, H. Ritsch, C. Genes, S. Hofer, G. D. Cole, W. Wiczorek, M. Arndt, T. Wilk for stimulating discussions and support and J. Schmöle for his graphical contributions. We acknowledge funding from the Austrian Science Fund FWF (START, SFB FOQUS), the European Commission (IP Q-ESSENCE, ITN cQOM), the European Research Council (ERC StG QOM), the John Templeton Foundation (RQ-8251) and the European Space Agency (AO/1-6889/11/NL/CBi). N. K. acknowledges support by the Alexander von Humboldt Stiftung. U. D., D. G. acknowledge support by the FWF through the Doctoral Programme CoQuS. R. K. acknowledges support from the Austrian Academy of Sciences (APART) and the European Commission (Marie Curie). M. A. and R. K. acknowledge support through the Keck Institute for Space Studies.

## Author Information

Correspondence and requests for materials should be addressed to N. K. (e-mail: nikolai.kiesel@univie.ac.at) or M. A. (e-mail: markus.aspelmeyer@univie.ac.at).

## Methods

### Loading of nanoparticles into the optical cavity trap

For our experiment we use silica nanospheres (Corpuscular Inc.) with a radius of  $r = 127 \pm 13$  nm, which are provided in an aqueous solution with a mass concentration of 10%. We dilute the solution with isopropanol to a mass concentration of  $10^{-7}$  and keep it for approximately 30 min in an ultrasonic bath before usage. To obtain airborne nanoparticles, an ultrasonic medical nebulizer (Omron Micro Air) emits droplets from the solution with approximately  $3\mu\text{m}$  size [48, 54]. On average, the number of nanospheres per droplet is then approximately  $5 \cdot 10^{-4}$ .

The nanospheres are loaded into the vacuum chamber by spraying the droplets through an inlet valve at the end of a 6mm thick, 90cm long steel tube. We keep the pressure inside the vacuum chamber between 1 and 5 mBar via manual control of both the inlet valve connected to the nebulizer and the outlet valve connected to the vacuum pumps. During the loading process, the trapping laser is kept resonant with the cavity at the desired intracavity power for optical trapping. The low

pressure minimizes pressure-induced fluctuations of the optical path length, which significantly simplifies locking the laser to the cavity.

Trapping in the conservative potential of the standing-wave trap is only possible with an additional dissipative process, which is provided fully by damping due to the remaining background gas. Within a few seconds after opening the valve, nanospheres get optically trapped. The standing-wave configuration provides multiple trapping positions. Trapped nanoparticles are detected by a CCD-camera, which is also used to determine their position  $x_0$  (see appendix E). If initially more than one position in the cavity is occupied, blocking the trapping beam for short intervals allows losing surplus particles for our measurements. To move the trapped particle to different positions along the cavity, we blue-detune the control laser to heat the CM degree of freedom of the particle. The “hot” particle moves across the standing wave until the control beam is switched off and the particle stays trapped at its new position (see Figure 2b).

### Readout of control beam

For the position readout of the nanoparticle motion, we rely on the dispersive interaction with the control-field cavity mode. The control laser beam is initially prepared with a frequency difference of  $\delta\omega \approx 2\pi \times 13.67$  GHz with respect to the original laser frequency  $\omega_0$ . When the

control beam is transmitted through the cavity, it experiences a phase shift according to its detuning from the resonance  $\omega_{cav}$ . Because the particle position in the cavity modifies the cavity resonance frequency  $\omega_{cav}$ , a phase readout of the transmitted control beam allows reconstructing the nanoparticle’s motion. To detect the phase modulation introduced by the particle motion along the cavity, we first mix the control beam with a local oscillator (LO, 3.15 mW; control beam power  $< 0.1$  mW) at frequency  $\omega_0$  at PBS5 (Fig. 1). In the output ports of PBS5, we then detect the optical signal at photodetectors PD1 and PD2 (Discovery Semiconductor Inc. DSCR410), which are fast enough to process the beat signal at frequency  $\delta\omega$ . Their difference signal  $l(t)$ , i.e., the heterodyne measurement outcome, contains the beat signal, whose phase  $\phi_{opt}$  is determined by the unknown path difference between the LO and the control beam. The beat signal carries sidebands representing the amplitude and phase modulation imprinted on the control beam by the optomechanical system. We demodulate  $l(t)$  with an electronic local oscillator (ELO) with frequency  $\delta\omega$  and phase  $\phi_{ELO}$  (relative to the beat signal). From the resulting signal  $s_{opt}(t)$ , we extract the phase modulation of  $l(t)$  by adjusting  $\phi_{ELO}$  such that the total phase  $\phi_{ELO} + \phi_{opt} = \pi/2$ . This is achieved by locking the DC part of  $\langle s_{opt}(t) \rangle$  to zero. We record the NPS of  $s_{opt}(t)$  with a spectrum analyzer, which allows reconstructing the NPS of the nanoparticle’s motion in post processing.

## Appendix A: Description of the Optomechanical System

### Optomechanical Hamiltonian

To describe our experiment theoretically, we consider a nanoparticle that is optically trapped within a Fabry-Perot cavity. Two laser beams drive adjacent TEM<sub>00</sub> cavity modes. One beam is used for optical trapping (trapping beam), the other for optomechanical control and readout of the nanoparticle center-of-mass motion (control beam). The two mode’s resonance frequencies differ by one FSR =  $\frac{c}{2L}$  ( $L$ : cavity length). In the most general case, the two lasers can be detuned from the respective cavity resonance frequency by  $\Delta_t$  and  $\Delta_c$  ( $\Delta_{c(t)}$ : detuning of the control (trapping) beam). The system is described using the following Hamiltonian [48]:

$$\begin{aligned} \hat{H}/\hbar = & \Delta_t \hat{a}_t^\dagger \hat{a}_t + \Delta_c \hat{a}_c^\dagger \hat{a}_c + \frac{\hat{p}_m^2}{2m\hbar} - U_0 \hat{a}_t^\dagger \hat{a}_t \sin^2(k_t \hat{x}) \\ & - U_0 \hat{a}_c^\dagger \hat{a}_c \sin^2(k_c \hat{x}) + iE_t(\hat{a}_t^\dagger - \hat{a}_t) + iE_c(\hat{a}_c^\dagger - \hat{a}_c), \end{aligned} \quad (\text{A1})$$

where  $U_0$  can be understood as the cavity resonance frequency shift introduced by a nanoparticle that is located at the intensity maximum at the center of the optical cavity. At the same time,  $\hbar U_0$  is also the trap depth created by a single intracavity photon ( $\hat{a}_{c(t)}^\dagger / \hat{a}_{c(t)}$ : creation/annihilation operator of the control (trapping) field in the cavity;  $m$ : mass of the nanoparticle;  $\hat{x}$  ( $\hat{p}_m$ ): position (momentum) operator of the nanoparticle’s CM;  $k_{c(t)}/E_{c(t)}$ : wavenumber/driving field of the control (trapping) beam).

Given  $|k_t - k_c| \ll k_c$ , one can regard  $(k_t - k_c)\hat{x}$  as a position-dependent phase shift between the standing waves of the two intracavity fields via  $\sin^2(k_t \hat{x}) = \sin^2(k_c \hat{x} + (k_t - k_c)\hat{x}) = \sin^2(k_c \hat{x} + \varphi)$ , where

$$\varphi = (k_t - k_c)x'_0 = \frac{2\pi \text{FSR}}{c} x'_0 = \frac{\pi}{L} x'_0$$

We include the dependence on  $k_t$  in  $\varphi$  and use  $k$  instead of  $k_c$  from this point on. Further, we rewrite the position operator  $\hat{x}$  as the sum of three terms:  $\hat{x} = x'_0 + \bar{x} + \hat{x}_m$ , where  $x'_0$  is the position of the intensity maximum of the

control field with respect to the cavity mirror ( $\bar{x}$ : the nanoparticle's mean displacement from  $x'_0$ ,  $\hat{x}_m$ : the nanoparticle's displaced position operator with  $\langle \hat{x}_m \rangle = 0$ ). Note that in the main text we always use the distance from the cavity center  $x_0$ , where  $x'_0 = x_0 + L/2$ . We also introduce the dimensionless position operator  $\delta\hat{x}$  with  $\hat{x}_m = X_{\text{gs}} \cdot \delta\hat{x}$ , where  $\delta\hat{x} = \frac{1}{\sqrt{2}}(\hat{b} + \hat{b}^\dagger)$  ( $X_{\text{gs}}$ : Ground state extension of the mechanical oscillator,  $b^{(\dagger)}$ : CM-motion annihilation (creation) operator).

We approximate the trigonometric functions in equation A1 to a second-order in  $\hat{x}_m$  and perform a displacement operation of the light operators:  $\hat{a}_j \rightarrow \alpha_j + \hat{a}_j$  about their steady-state mean values  $\alpha_t$  and  $\alpha_c$ . The Hamiltonian after these modifications is:

$$\begin{aligned} \frac{H}{\hbar} &= \Delta_t |\alpha_t|^2 + \Delta_c |\alpha_c|^2 + \Delta_t \alpha_t (\hat{a}_t + \hat{a}_t^\dagger) + \Delta_c \alpha_c (\hat{a}_c + \hat{a}_c^\dagger) + \Delta_t \hat{a}_t^\dagger \hat{a}_t + \Delta_c \hat{a}_c^\dagger \hat{a}_c \\ &+ \frac{\hat{p}_m^2}{2m\hbar} - U_0 |\alpha_t|^2 \sin^2(k(x'_0 + \bar{x}) + \varphi) - U_0 |\alpha_c|^2 \sin^2(k(x'_0 + \bar{x})) \\ &- 2U_0 k^2 |\alpha_t|^2 \cos(2k(x'_0 + \bar{x}) + 2\varphi) \frac{\hat{x}_m^2}{2} - 2U_0 k^2 |\alpha_c|^2 \cos(2k(x'_0 + \bar{x})) \frac{\hat{x}_m^2}{2} \\ &- U_0 k \alpha_t \sin(2k(x'_0 + \bar{x}) + 2\varphi) (\hat{a}_t + \hat{a}_t^\dagger) \hat{x}_m - U_0 k \alpha_c \sin(2k(x'_0 + \bar{x})) (\hat{a}_c + \hat{a}_c^\dagger) \hat{x}_m \\ &- U_0 |\alpha_t|^2 k \sin(2k(x'_0 + \bar{x}) + 2\varphi) \hat{x}_m - U_0 |\alpha_c|^2 k \sin(2k(x'_0 + \bar{x})) \hat{x}_m \\ &- U_0 \alpha_t \sin^2(k(x'_0 + \bar{x}) + \varphi) (\hat{a}_t + \hat{a}_t^\dagger) - U_0 \alpha_c \sin^2(k(x'_0 + \bar{x})) (\hat{a}_c + \hat{a}_c^\dagger) \\ &+ iE_t (\hat{a}_t^\dagger - \hat{a}_t) + iE_c (\hat{a}_c^\dagger - \hat{a}_c). \end{aligned} \quad (\text{A2})$$

Line A2 takes the form of a harmonic potential  $\frac{m\Omega_0^2 \hat{x}_m^2}{2\hbar}$  with mechanical frequency  $\Omega_0$ :

$$\Omega_0^2 = -\frac{2\hbar U_0 k^2}{m} (|\alpha_t|^2 \cos(2k(x'_0 + \bar{x}) + 2\varphi) + |\alpha_c|^2 \cos(2k(x'_0 + \bar{x}))). \quad (\text{A3})$$

Line A2 determines the linear dispersive coupling of the nanosphere CM motion to the trapping and cooling beam. Note that the trapping beam also shows linear coupling when the cooling beam is strong enough to significantly contribute to the optical trap:

$$\begin{aligned} g_{0,t} &= \zeta_t \cdot X_{\text{gs}} = U_0 k X_{\text{gs}} \sin 2(k(x'_0 + \bar{x}) + \varphi) \\ g_{0,c} &= \zeta_c \cdot X_{\text{gs}} = U_0 k X_{\text{gs}} \sin 2k(x'_0 + \bar{x}). \end{aligned} \quad (\text{A4})$$

Note that we use  $g_0 = g_{0,c}$  in the main text. To study the dynamics of the system, we solve the Langevin equations for both light fields:

$$\begin{aligned} \dot{\hat{a}}_t &= -\left(\frac{\kappa}{2} + i(\Delta_t - U_0 \sin^2(k(x'_0 + \bar{x}) + \varphi))\right) (\hat{a}_t + \alpha_t) + E_t - \zeta_t \alpha_t \hat{x}_m \\ \dot{\hat{a}}_c &= -\left(\frac{\kappa}{2} + i(\Delta_c - U_0 \sin^2 k(x'_0 + \bar{x}))\right) (\hat{a}_c + \alpha_c) + E_c - \zeta_c \alpha_c \hat{x}_m \end{aligned} \quad (\text{A5})$$

The additional loss terms account for the cavity amplitude decay rate  $\kappa$ . The value of  $\kappa$  is assumed to be equal for both light fields due to the small difference in their wavelengths. For the steady-state solutions of  $\hat{a}_t$  and  $\hat{a}_c$  we find:

$$\begin{aligned} \alpha_t &= \frac{E_t}{\frac{\kappa}{2} + i(\Delta_t - U_0 \sin^2 k(x'_0 + \bar{x}) + \varphi)} \\ \alpha_c &= \frac{E_c}{\frac{\kappa}{2} + i(\Delta_c - U_0 \sin^2(k(x'_0 + \bar{x})))}. \end{aligned} \quad (\text{A6})$$

In our experiment, the Pound-Drever-Hall feedback loop keeps the trapping-laser frequency resonant to the corresponding cavity resonance frequency when the particle is in its steady state position. In other words, the detuning  $\Delta_t$  compensates the frequency shift caused by the particle such that  $\Delta_t - U_0 \sin^2(k(x'_0 + \bar{x}) + \varphi) = 0$ .

On the other hand, the frequency of the control beam is varied throughout the experiment. We are interested in the detuning  $\Delta$  of the control beam with respect to the cavity resonance when the nanoparticle is located at its steady state position:  $\Delta = \Delta_c - U_0 \sin^2 k(x'_0 + \bar{x})$ .

The trapping beam power is not changed throughout the experiment. In contrast, the control beam power is always set to achieve the desired ratio between the power of the two intracavity fields  $\mu$ :

$$\mu = \frac{|\alpha_c|^2}{|\alpha_t|^2} = \frac{|E_c|^2}{|E_t|^2} \frac{\left(\frac{\kappa}{2}\right)^2}{\left(\frac{\kappa}{2}\right)^2 + \Delta^2}. \quad (\text{A7})$$

Heisenberg's equation of motion for the particle becomes:

$$\ddot{\hat{x}}_m + \Omega_0^2(\mu)\hat{x}_m = \frac{\hbar k U_0}{m} [|\alpha_t|^2 \sin 2(k(x'_0 + \bar{x}) + \varphi) + |\alpha_c|^2 \sin 2k(x'_0 + \bar{x})] - \gamma_m \dot{\hat{x}}_m \quad (\text{A8})$$

where we included an additional damping term  $\gamma_m \dot{\hat{x}}_m$ , which is due to the collisions of the nanoparticle with the surrounding gas.

From Equation A8 we find a steady state condition on  $x'_0 + \bar{x}$ , that enables us to determine the mechanical frequency  $\Omega_0$  and the displacement  $\bar{x}$  as a function of  $\mu$ :

$$\begin{aligned} \Omega_0^2(\mu) &= \Omega_0^2(0) \sqrt{1 + \mu^2 + 2\mu \cos 2\varphi} \\ \tan 2k\bar{x} &= -\frac{\sin 2\varphi}{\mu + \cos 2\varphi}. \end{aligned} \quad (\text{A9})$$

Thereby, the mechanical frequency in absence of the cooling beam is (equation A3):

$$\Omega_0^2(0) = \frac{2\hbar U_0 k^2}{m} |\alpha_t|^2.$$

Note that the case of a control beam that significantly contributes to the optical trap that has been presented here has also already been published in [47, 48].

### Cavity mode shape

Up to this point, we have neglected the mode shape of the TEM00 cavity mode (Fig. 2a, main text). The waist of the mode, however, depends on the position  $x_0$  in the cavity. The maximum intensity of the standing wave along the TEM00 mode in the cavity is, accordingly, position dependent [55]:

$$I(x_0) = I_0 \frac{1}{1 + \frac{x_0^2}{x_R^2}},$$

note, that we have used here  $x_0$  as the distance from the center of the cavity. It is related to the distance from the mirror  $x'_0$  by  $x_0 = x'_0 - \frac{L}{2}$  ( $x_R$ : Rayleigh length of the mode). Therefore,  $U_0$  is an explicit function of the trap position  $x_0$ :

$$U_0(x_0) = \frac{\omega_{cav} \xi}{2\varepsilon_0 V_c} \left(1 + \frac{x_0^2}{x_R^2}\right)^{-1},$$

( $\omega_{cav}$ : laser frequency,  $\xi$ : particle polarizability,  $\varepsilon_0$ : vacuum permittivity,  $V_c$ : cavity mode volume). The polarizability of a particle is (see e.g. [13]):

$$\xi = 4\pi r^3 \varepsilon_0 \operatorname{Re} \left( \frac{\varepsilon - 1}{\varepsilon + 2} \right)$$

( $\varepsilon$ : nanoparticle's dielectric constant;  $r$ : particle radius). In the main text we use these equations to determine the estimated particle size from  $U_0(x_0)$ , which is determined from the control beam power dependent coupling  $g_0$  (see main text, figure 3d) and the independently determined position of a particle in the cavity  $x_0$  (see appendix E).

### Langevin Equations, effective frequency and damping

The Langevin equations for the mechanical quantum harmonic oscillator coupled to a thermal bath are:

$$\begin{aligned} \dot{\hat{x}}_m &= \frac{\hat{p}_m}{m} \\ \dot{\hat{p}}_m &= -m\Omega_0^2 \hat{x}_m - \gamma_m \hat{p}_m + \sum_{j=t,c} \hbar \zeta_j \alpha_j (\hat{a}_j^\dagger + \hat{a}_j) + \eta(t), \end{aligned} \quad (\text{A10})$$

where  $\eta(t)$  is a thermal noise term, with the following correlation property [56]:

$$\langle \eta(t)\eta(t') \rangle = \frac{\gamma_m}{\Omega_0} \int \frac{d\omega}{2\pi} e^{-i\omega(t-t')} \omega \coth\left(\frac{\hbar\omega}{2k_B T}\right).$$

We assume that we are in a temperature range where  $k_B T/\hbar \gg \Omega_0$ :

$$\langle \eta(t)\eta(t') \rangle = \gamma_m \frac{2k_B T}{\hbar\Omega_0} \delta(t-t').$$

For the light beams, we can use the equations of motion as provided in equation A5 after the displacement of the light operators:

$$\begin{aligned} \dot{\hat{a}}_c &= -\left(\frac{\kappa}{2} + i\Delta\right)\hat{a}_c + i\zeta_c \alpha_c \hat{x}_m + \sqrt{\kappa}(\hat{c}_c^{in} + \hat{d}_c^{in}), \\ \dot{\hat{a}}_t &= -\frac{\kappa}{2}\hat{a}_t + i\zeta_t \alpha_t \hat{x}_m + \sqrt{\kappa}(\hat{c}_t^{in} + \hat{d}_t^{in}) \end{aligned} \quad (\text{A11})$$

By Fouriertransformation, we obtain a linear system of equations from which we retrieve the final expression for the position spectrum  $S_{xx}(\omega)$  of levitating nanoparticles CM motion:

$$S_{xx} = |\chi_m^{\text{eff}}|^2 [S_{\text{th}} + S_{\text{rp}}],$$

where  $S_{\text{th}}$  is the thermal noise contribution and  $S_{\text{rp}}$  is the radiation-pressure contribution. In the regime our experiment is currently operating ( $T = 293$  K; air pressure approx. 1-5 mbar), we expect that the thermal-noise contribution prevales:

$$S_{\text{th}} = X_{gs}^2 \gamma_m \frac{2k_B T}{\hbar\Omega_0}$$

The effective susceptibility of the mechanical oscillator is

$$\chi_m^{\text{eff}} = \frac{\gamma_m}{(\Omega_{\text{eff}}(\omega)^2 - \omega^2)^2 - i\gamma_{\text{eff}}(\omega)^2 \omega^2}, \quad (\text{A12})$$

where, following [56], we used the expressions:

$$\begin{aligned} \gamma_{\text{eff}}(\omega) &= \gamma_m - \frac{4g_0^2 |\alpha_c|^2 \Omega_0(\mu) \Delta \frac{\kappa}{2}}{\left(\left(\frac{\kappa}{2}\right)^2 + (\omega + \Delta)^2\right) \left(\left(\frac{\kappa}{2}\right)^2 + (\omega - \Delta)^2\right)} \\ \Omega_{\text{eff}}(\omega) &= \left[ \Omega_0^2(\mu) + \frac{2g_0^2 |\alpha_c|^2 \Omega_0(\mu) \Delta \left[\left(\frac{\kappa}{2}\right)^2 - \omega^2 + \Delta^2\right]}{\left(\left(\frac{\kappa}{2}\right)^2 + (\omega + \Delta)^2\right) \left(\left(\frac{\kappa}{2}\right)^2 + (\omega - \Delta)^2\right)} \right]^{1/2}. \end{aligned}$$

## Appendix B: Position readout by homodyne detection of the control beam

The expressions for the mechanical oscillator's dynamics, as well as its relationship to the control beam in the cavity, have been derived in the previous section (equations A10 and A11). In the following two sections, we will discuss how the mechanical oscillator position NPS is determined from the NPS obtained by homodyning of the control-beam phase signal in transmission of the cavity (see Methods M2 for implementation of homodyne detection).

We first derive the control light field in cavity transmission via the cavity input-output relation [57]:

$$\hat{d}_c^{\text{out}}(t) = \sqrt{\kappa} \hat{a}_c(t) - \hat{d}_c^{\text{in}}(t), \quad (\text{B1})$$

where  $\hat{d}_c^{\text{in}}$  describes the quantum noise at the cavity back mirror (i.e., the side from which the cavity is not driven). Even though our detection scheme occurs in two steps as described in the methods section, it is completely equivalent to a standard homodyne detection. The output signal is accordingly described by [58]:

$$s_{\text{opt}}(t) = \frac{1}{2} \left( |\hat{d}_c^{\text{out}} + \hat{a}_{LO}|^2 - |\hat{d}_c^{\text{out}} - \hat{a}_{LO}|^2 \right) = \hat{d}_c^{\text{out}} \hat{a}_{LO}^* + \hat{d}_c^{\text{out}\dagger} \hat{a}_{LO}, \quad (\text{B2})$$

where we describe the local oscillator by  $\hat{a}_{LO}(t) = \alpha_{LO} \cdot e^{-i(\omega_c t + \theta)}$ , where  $\theta$  determines the detected quadrature of the control beam and  $\alpha_{LO}$  is assumed to be real. In our experiment, the readout phase is locked to measure the phase quadrature:  $\theta = \frac{\pi}{2}$ .

From equations B1 and B2 we obtain:

$$\langle |\tilde{s}_{\text{opt}}(\omega)|^2 \rangle = \kappa \zeta_c^2 \alpha_c^2 |\chi_c(\omega) + \chi_c^*(-\omega)|^2 S_{xx}(\omega) \delta(\omega), \quad (\text{B3})$$

where we used the cavity susceptibility  $\chi_c(\omega) = \frac{1}{\frac{\omega}{2} - i(\omega - \Delta)}$ . Up to a proportionality factor, Equation B3 resembles the result of the detection described in [49], and allows us to derive the mechanical NPS  $S_{xx}(\omega)$  from the detected signal.

### Appendix C: Data Evaluation and Temperature Calibration

To extract the mechanical NPS, we first measure the spectrum of the homodyne phase readout with and without particle for all values of  $\mu$  and  $\Delta$ . We obtain  $\langle |\tilde{s}_{\text{opt}}(\omega)|^2 \rangle$  by subtracting the background NPS (without particle) from the NPS with particle. To reconstruct the mechanical NPS  $S_{xx}$ , we need to account for the filtering by the Fabry-Perot cavity. We therefore divide  $\langle |\tilde{s}_{\text{opt}}(\omega)|^2 \rangle$  by  $|\chi_c(\omega) + \chi_c^*(-\omega)|^2$  following equation B3. The exact shape of  $S_{xx}$  is given by equation A12. To determine the effective frequency, damping and temperature we assume that we can describe the CM-motion of the particle as an harmonic oscillator, which is fulfilled as we are not operating in the strong coupling regime:

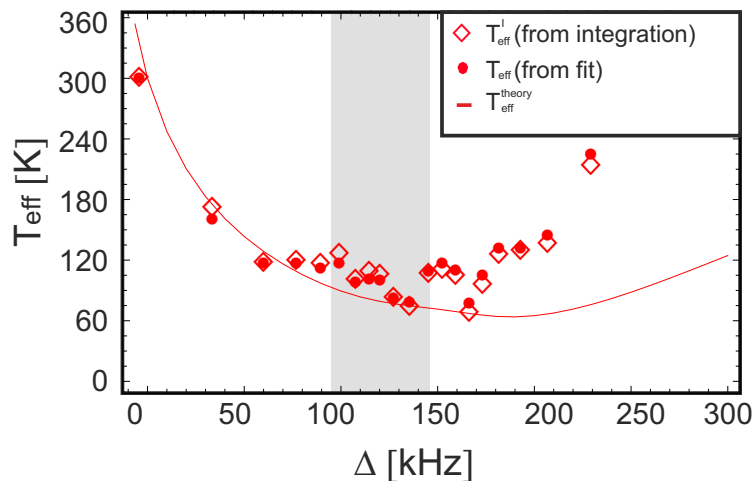


FIG. 4: **CM-motion temperature as a function of detuning.** The temperature of the CM-motion along the cavity axis as a function of detuning. The values are inferred via the equipartition theorem from the direct integration of the NPS ( $T_{\text{eff}}^I$ , solid circles) and from the fitted spectra ( $T_{\text{eff}}^*$ , empty diamonds). The solid line shows the theoretical expectation  $T_{\text{eff}}^{\text{theory}}(\Delta)$  inferred from the detuning dependent frequency fit (optical spring; main text, Fig. 3).

$$f(\omega) = a \cdot T_{\text{eff}} \cdot \frac{\gamma_m}{(\omega^2 - \Omega_{\text{eff}}^2)^2 + \omega^2 \gamma_{\text{eff}}^2}. \quad (\text{C1})$$

By fitting this model to  $S_{xx}$ , we obtain  $\gamma_{\text{eff}}$ ,  $\Omega_{\text{eff}}$  and  $T_{\text{eff}}^*$ . The calibration constant  $a$  is determined such that  $T_{\text{eff}} = 293\text{K}$  in a particular measurement that was performed close to zero detuning ( $\Delta = 1$  kHz for  $\mu = 0.4$ , blue NPS in Fig. 3, main text). This results in the values for the optical spring  $\Omega_{\text{eff}}$  and damping  $\gamma_{\text{eff}}$  in Fig. 3, main text.

We can determine the optomechanical coupling  $g_0$  from the the detuning dependence of  $\Omega_{\text{eff}}$  for a given value of  $\mu$ . However, we do not have an explicit analytical expression for this dependence. Instead, we apply the following strategy:

Using equation A12, we can calculate the optomechanical NPS  $S_{xx}^{\text{theory}}$  of our system for a given set of parameters ( $\kappa$ ,  $g_0$ ,  $\Omega_0$  and  $\delta\Delta$ ). Here,  $\delta\Delta$  is a systematic deviation from the detuning we set in the measurement: each value of  $\Delta$  can be set precisely up to the uncertainty in the actual cavity resonance frequency. This frequency difference is accounted for with a joint offset  $\delta\Delta$  in the values of  $\Delta$  that is used as a fit parameter. We treat  $S_{xx}^{\text{theory}}$  in the same manner as the data and extract  $\gamma_{\text{eff}}^{\text{theory}}$ ,  $\Omega_{\text{eff}}^{\text{theory}}$  and  $T_{\text{eff}}^{\text{theory}}$  by fitting  $f(\omega)$  for each value of  $\Delta$ . We use  $\Omega_{\text{eff}}^{\text{theory}}(\Delta)$

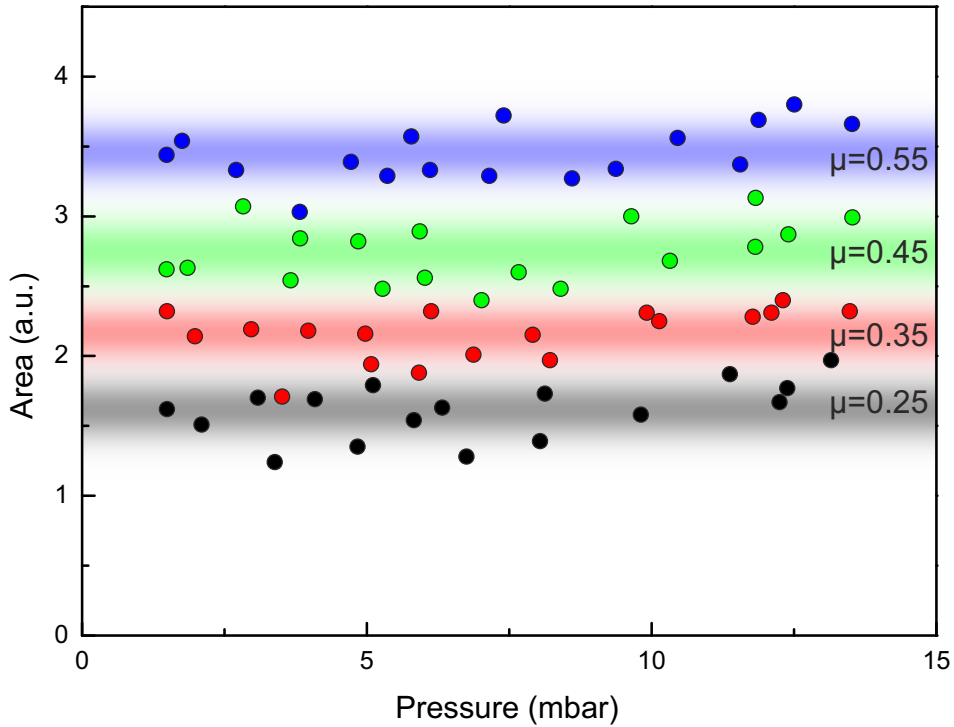


FIG. 5: Measurement of the NPS-area as a function of the ambient pressure. The data were taken for a resonant control beam. The area is proportional to the temperature of the CM motion of the nanoparticle for a given value of  $\mu$ . It is independent of pressure indicating that the CM motion of the trapped nanoparticles is thermalized with the surrounding gas over the full measurement range. We conclude that the effective temperature of the CM mode is room temperature (293 K). The scatter of the data corresponds to a standard deviation of 5% for a temperature that is inferred from the area of the NPS.

as a model that we fit to  $\Omega_{\text{eff}}$  optimizing the parameters  $g_0$ ,  $\Omega_0$  and  $\delta\omega$  in a least-square fit. The FWHM cavity line width  $\kappa$  is determined independently. The best fit parameters are used to obtain the theoretical dependences of  $\gamma_{\text{eff}}^{\text{theory}}$  and  $\Omega_{\text{eff}}^{\text{theory}}$  on the detuning shown in Fig. 3 in the main text and  $T_{\text{eff}}^{\text{theory}}$  shown in Fig. 4.

The corresponding values of the predicted effective temperatures  $T_{\text{eff}}^{\text{theory}}$  are shown in Fig. 4 along with the experimental data for  $\mu = 0.4$ . The latter is obtained in two ways: firstly as a free parameter  $T_{\text{eff}}^*$  in the fitted model  $f(\omega)$  and secondly by direct integration over the measured NPS via  $T_{\text{eff}}^I = a^I \Omega_{\text{eff}}^2 \int S_{xx} d\omega$ . The calibration factor  $a^I$  is derived in the same way as  $a$ . The values  $T_{\text{eff}}^*$ , obtained via fitting, agree well with those obtained by direct integration of the NPS. For small detunings  $\Delta$ , the data follows the theoretical curve, while for larger detunings, heating unaccounted for in the theoretical model seems to occur. We are still investigating this effect, which may be due to laser noise. To obtain a good estimate of the minimal temperature achieved experimentally, we average the temperature obtained for a range of detunings  $\Delta/2\pi \in [100, 150]$  kHz. The range is chosen such that the onset of temperature increase is not yet strong and the predicted range of  $T_{\text{eff}}$  is small compared to the distribution of measured temperatures. The experimental data in Fig. 3e in the main text is obtained by applying this evaluation for the different values of  $\mu$  for  $T_{\text{eff}}^I$  obtained by direct integration. The theory curve in Fig. 3e in the main text is obtained by averaging the theoretical prediction for  $T_{\text{eff}}^{\text{theory}}$  over the same range of detunings  $\Delta/2\pi \in [100, 150]$  kHz.

#### Appendix D: Kinetic gas theory - Pressure-dependent damping

The pressure dependence of the damping for a trapped nanosphere is given by [21, 22, 59] :

$$\gamma_0 = \frac{6\pi\eta r}{m} \frac{0.619}{0.619 + Kn} (1 + c_k) \quad (\text{D1})$$

where  $\eta$  is the viscosity coefficient for air,  $r$  and  $m$  are the radius and mass of the nanosphere,  $Kn = \lambda_{\text{fp}}/r$  is the Knudsen number and  $\lambda_{\text{fp}}$  is the mean free path for air particles.  $c_k = 0.31Kn/(0.785 + 1.152Kn + Kn^2)$  is a small

correction factor necessary at higher pressures [59]. Figure 2b in the main text shows a pressure dependent damping measurement, where the control beam is used just for readout (i.e.  $\mu=0.1$ , resonant).

Figure 5 shows the temperature associated with the CM motion of the particle as a function of pressure. At high pressures, the nanoparticle experiences more collisions with the gas resulting in a stronger damping of its CM motion. If the nanoparticle CM motion was not thermalized at low pressures due to a heating process, better thermalization and therefore lower temperatures would be expected at higher pressures due to the increased damping rate. As Fig. 5 shows a constant CM motion temperature for the different pressures and values of  $\mu$ , we conclude it is thermalized with the environment in all these measurements, which implies a temperature of 293K as long as no optical damping is introduced.

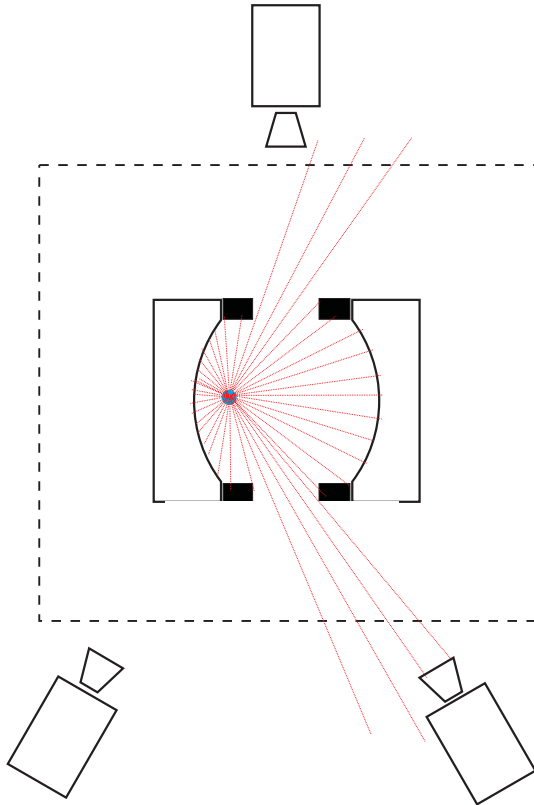


FIG. 6: **Schematic of the configuration of the CCD imaging setup.** We use a combination of three CCD cameras to observe and locate the particle. This configuration allows access to a larger range of positions along the cavity axis compared to a single camera. Based on the pictures of the CCD cameras, we determine the position  $x_0$  of a particle in the cavity.

### Appendix E: Position detection

Three cameras with achromatic lenses monitor the cavity and image the light scattered off trapped nanoparticles. As can be seen in Figure 1a of the main text, the black retaining rings and the concave shape of the mirrors prevent optical access over the whole cavity length from a single point of view. We use a configuration of three CCD cameras, as shown in figure 6, to extend the field of view. By combining the images from the 3 cameras, we can reconstruct a larger field of view. To determine the position of the particle from the image, we need to calibrate the coordinates. To this end, the mechanical frequency at several positions is measured along with the position of a particle on the CCD image. This measurement is repeated for several particles. The frequency dependence on position allows calibrating the camera.

The mode shape in the optical cavity is well-known from the curvature of the mirrors and the cavity length, which is determined with high precision from the FSR. The expected longitudinal frequency dependence of a nanoparticle trapped in the standing wave is  $\Omega_0 = \Omega_c \frac{1}{\sqrt{1+((x_0-x_c)/x_R)^2}}$  ( $x_c$ : cavity center position,  $\Omega_c$ : frequency at position  $x_c$ ;  $x_R$ : Rayleigh length of the Gaussian mode). The measured mechanical frequencies for several different trap

positions of the same nanoparticle and the corresponding coordinates  $\zeta$  (in pixels) on the camera images are fitted to the function  $\Omega_0 = \Omega_c \frac{1}{\sqrt{1 + ((\zeta - \zeta_c)\xi/x_R)^2}}$  with fit parameters  $\zeta_c$  (coordinate of the center of the cavity in pixels),  $\xi$  (conversion factor between pixels and millimeters) and  $\Omega_c$  (mechanical frequency in the center of the cavity). A corresponding measurement for one nanoparticle with calibrated length scale is shown in the main text, figure 2b. Based on this calibration we determine the position of the nanoparticle used in the measurements summarized in Fig. 3. It is located at a distance  $x'_0 = 3.92 \pm 0.14$  mm from the cavity mirror, i.e. at a distance  $x_0 = 1.56 \pm 0.14$  mm from the center of the cavity.

- 
- [1] R. Blatt and C. F. Roos, *Nature Physics* **8**, 277 (2012).
  - [2] I. Bloch, J. Dalibard, and S. Nascimbène, *Nature Physics* **8**, 267 (2012).
  - [3] H. Häffner, R. C., and R. Blatt, *Physics Reports* **469**, 155 (2008).
  - [4] D. Kielpinski, C. Monroe, and D. J. Wineland, *Nature* **417**, 709 (2002).
  - [5] H. J. Kimble, *Nature* **453**, 1023 (2008).
  - [6] S. Ritter, C. Nölleke, C. Hahn, A. Reiserer, A. Neuzner, M. Uphoff, M. Mücke, E. Figueroa, J. Bochmann, and G. Rempe, *Nature* **484**, 195 (2012).
  - [7] A. Stute, B. Casabone, B. Brandstatter, K. Friebe, T. E., Northup, and R. Blatt, *Nat Photon* **7**, 219 (2013).
  - [8] J. Hofmann, M. Krug, N. Ortegel, L. Gérard, M. Weber, W. Rosenfeld, and H. Weinfurter, *Science* **337**, 72 (2012).
  - [9] S. Gerlich, S. Eibenberger, M. Tomandl, S. Nimmrichter, K. Hornberger, P. J. Fagan, J. Tüxen, M. Mayor, and M. Arndt, *Nature Communications* **2**, 263 (2011).
  - [10] K. Hornberger, S. Gerlich, P. Haslinger, S. Nimmrichter, and M. Arndt, *Reviews of Modern Physics* **84**, 157 (2012).
  - [11] M. Aspelmeyer, P. Meystre, and K. Schwab, *Physics Today* **65**, 29 (2012).
  - [12] M. Aspelmeyer, T. Kippenberg, and F. Marquardt, arXiv:1303.0733v1 (2013).
  - [13] D. E. Chang, C. A. Regal, S. B. Papp, D. J. Wilson, J. Ye, O. Painter, H. J. Kimble, and P. Zoller, *Proceedings of the National Academy of Sciences of the United States of America* **107**, 1005 (2010).
  - [14] O. Romero-Isart, M. L. Juan, R. Quidant, and J. I. Cirac, *New Journal of Physics* **12**, 033015 (2010).
  - [15] O. Romero-Isart, A. C. Pflanzer, F. Blaser, R. Kaltenbaek, N. Kiesel, M. Aspelmeyer, and J. I. Cirac, *PRL* **107**, 020405 (2011).
  - [16] A. Geraci, S. Papp, and J. Kitching, *Phys. Rev. Lett.* **105**, 101101 (2010).
  - [17] A. Arvanitaki and A. A. Geraci, *Phys. Rev. Lett.* **110**, 071105 (2013).
  - [18] P. Horak, G. Hechenblaikner, K. Gheri, H. Stecher, and H. Ritsch, *Physical Review Letters* **79**, 4974 (1997).
  - [19] V. Vuletić and S. Chu, *Physical Review Letters* **84**, 3787 (2000).
  - [20] A. Ashkin and J. M. Dziedzic, *Applied Physics Letters* **30**, 202 (1977).
  - [21] T. Li, S. Kheifets, and M. G. Raizen, *Nat Phys* **7**, 527 (2011).
  - [22] J. Gieseler, B. Deutsch, R. Quidant, and L. Novotny, *Physical Review Letters* **109**, 103603 (2012).
  - [23] M. Koch, C. Sames, A. Kubanek, M. Apel, M. Balbach, A. Ourjoumtsev, P. Pinkse, and G. Rempe, *Physical Review Letters* **105**, 173003 (2010).
  - [24] J. Ye, D. W. Vernooy, and H. J. Kimble, *Physical Review Letters* **83**, 4987 (1999).
  - [25] J. McKeever, J. R. Buck, A. D. Boozer, A. Kuzmich, H.-C. Nägerl, D. M. Stamper-Kurn, and H. J. Kimble, *Physical Review Letters* **90**, 2 (2003).
  - [26] P. Maunz, T. Puppe, I. Schuster, N. Syassen, P. W. H. Pinkse, and G. Rempe, *Nature* **428**, 50 (2004).
  - [27] D. R. Leibbrandt, J. Labaziewicz, V. Vuletic, and I. L. Chuang, *Phys. Rev. Lett.* **103**, 103001 (2009).
  - [28] A. Stute, B. Casabone, P. Schindler, T. Monz, P. O. Schmidt, B. Brandstatter, T. E. Northup, and R. Blatt, *Nature* **485**, 482 (2012).
  - [29] G. Hechenblaikner, M. Gangl, P. Horak, and H. Ritsch, *Physical Review A* **58**, 3030 (1998).
  - [30] M. Gangl and H. Ritsch, *European Physical Journal D* **8**, 29 (2000).
  - [31] I. Favero, S. Stapfner, D. Hunger, P. Paulitschke, J. Reichel, H. Lorenz, E. M. Weig, and K. Karrai, *Optics Express* **17**, 16 (2009).
  - [32] G. Anetsberger, O. Arcizet, Q. P. Unterreithmeier, R. Rivière, A. Schliesser, E. M. Weig, Kotthaus, J. P., and T. J. Kippenberg, *Nature Physics* **5**, 909 (2009).
  - [33] J. Chan, T. P. M. Alegre, A. H. Safavi-Naeini, J. T. Hill, A. Krause, S. Gröblacher, M. Aspelmeyer, and O. Painter, *Nature* **478**, 89 (2011).
  - [34] J. D. Thompson, B. M. Zwickl, A. M. Jayich, F. Marquardt, S. M. Girvin, and J. G. E. Harris, *Nature* **452**, 72 (2008).
  - [35] J. D. Teufel, T. Donner, D. Li, J. W. Harlow, M. S. Allman, K. Cicak, A. J. Sirois, J. D. Whittaker, K. W. Lehnert, and R. W. Simmonds, *Nature* **475**, 359 (2011).
  - [36] T. P. Purdy, R. W. Peterson, and C. A. Regal, *Science* **339**, 801 (2013).
  - [37] A. H. Safavi-Naeini, J. Chan, J. T. Hill, T. P. Mayer Alegre, A. Krause, and O. Painter, *Phys. Rev. Lett.* **108**, 033602 (2012).
  - [38] K. W. Murch, K. L. Moore, S. Gupta, and D. M. Stamper-Kurn, *Nature Physics* **4**, 561 (2008).
  - [39] T. Purdy, D. Brooks, T. Botter, N. Brahms, Z.-Y. Ma, and D. M. Stamper-Kurn, *Phys. Rev. Lett.* **105**, 133602 (2010).

- [40] M. H. Schleier-Smith, I. D. Leroux, H. Zhang, M. A. Van Camp, and V. Vuletić, *Physical Review Letters* **107**, 143005 (2011).
- [41] R. Kaltenbaek, G. Hechenblaikner, N. Kiesel, O. Romero-Isart, K. Schwab, U. Johann, and M. Aspelmeyer, *Experimental Astronomy* **34**, 123 (2012).
- [42] A. Ashkin, *Optical trapping and manipulation of neutral particles using lasers* (World Scientific Pub Co, 2007).
- [43] S. Nimmrichter, K. Hammerer, P. Asenbaum, H. Ritsch, and M. Arndt, *New Journal of Physics* **12**, 083003 (2010).
- [44] O. Romero-Isart, A. Pflanzner, M. Juan, R. Quidant, N. Kiesel, M. Aspelmeyer, and J. I. Cirac, *Phys. Rev. A* **83**, 013803 (2011).
- [45] P. F. Barker and M. N. Shneider, *Phys. Rev. A* **81**, 023826 (2010).
- [46] D. Stamper-Kurn, arXiv:1204.4351v1 (2012).
- [47] G. A. T. Pender, P. F. Barker, F. Marquardt, J. Millen, and T. S. Monteiro, *Phys. Rev. A* **85**, 021802 (2012).
- [48] T. S. Monteiro, J. Millen, G. A. T. Pender, F. Marquardt, D. Chang, and P. F. Barker, *New Journal of Physics* **15**, 015001 (2013).
- [49] M. Paternostro, S. Gigan, M. S. Kim, F. Blaser, H. R. Böhm, and M. Aspelmeyer, *New Journal of Physics* **8**, 107 (2006).
- [50] A. Ashkin and J. M. Dziedzic, *Applied Physics Letters* **28**, 333 (1976).
- [51] U. Akram, N. Kiesel, M. Aspelmeyer, and G. J. Milburn, *New Journal of Physics* **12**, 083030 (2010).
- [52] O. Romero-Isart, *Phys. Rev. A* **84**, 052121 (2011).
- [53] W. Lechner, S. J. M. Habraken, N. Kiesel, M. Aspelmeyer, and P. Zoller, *Phys. Rev. Lett.* **110**, 143604 (2013).
- [54] M. D. Summers, D. R. Burnham, and D. McGloin, *Optics Express* **16**, 7739 (2008).
- [55] B. E. A. Saleh and M. C. Teich, *Fundamentals of photonics* (Wiley-Interscience, 2007).
- [56] C. Genes, D. Vitali, P. Tombesi, S. Gigan, and M. Aspelmeyer, *Physical Review A* **77**, 33804 (2008).
- [57] C. Gardiner and P. Zoller, *Quantum noise: a handbook of Markovian and non-Markovian quantum stochastic methods with applications to quantum optics*, vol. 56 (Springer, 2004).
- [58] H.-A. Bachor and T. C. Ralph, *A Guide to Experiments in Quantum Optics* (Wiley-VCH, 2004).
- [59] S. A. Beresnev, V. G. Chernyak, and G. A. Fomyagin, *Journal of Fluid Mechanics* **219**, 405 (1990).